JOURNAL OF GEOPHYSICAL RESEARCH, VOL. 114, D20119, doi:10.1029/2008JD011441, 2009

Cross-equatorial influences of submonthly scale southerly surges over the eastern Indian Ocean during Southern Hemisphere winter

Yoshiki Fukutomi[1] and Tetsuzo Yasunari[1,2]

Received 8 November 2008; revised 8 July 2009; accepted 6 August 2009; published 31 October 2009.

[1] Lower-tropospheric southerly surges occurring at submonthly timescales over the eastern Indian Ocean (EIO) during Southern Hemisphere (SH) winter are extratropical-tropical interaction phenomena involving various processes. This study examined the physical mechanism driving equatorial wave disturbances associated with surge-induced cross-equatorial flow over the EIO. Japanese 25-Year Reanalysis (JRA25) and Tropical Rainfall Measuring Mission Satellite (TRMM) 3B42 data products from June to August for the 7 years from 1998 to 2004 were analyzed. Composite analyses of low-level wind and vorticity fields reveal that an equatorial clockwise gyre develops just after cross-equatorial penetration of southerly surge winds. This gyre is interpreted as an equatorially trapped Rossby wave that develops asymmetrically around the equator in response to surge-induced cross-equatorial flow. Eddy vorticity budget analysis demonstrates the dynamic role of the southerly surge in the genesis of the equatorial clockwise gyre. The result indicates that an injection of negative absolute vorticity into the equatorial tropics due to both advective and convergent processes associated with the surge winds is primarily responsible for the gyre genesis. Cross-equatorial advection of basic state absolute vorticity by the surge (eddy) winds and vortex stretching by surge wind convergence are most effective in spinning up the equatorial clockwise gyre. Wave activity flux analysis further emphasizes that Rossby wave energy propagation from the SH extratropics into the equatorial EIO region is caused by the southerly surge. These dynamic diagnostics suggest that the southerly surge plays a lateral forcing role in exciting the equatorial wave disturbance over the EIO. Composite analyses of moisture flux and precipitation anomalies characterize the equatorial clockwise gyre as a convectively coupled equatorial Rossby wave. Enhanced cross-equatorial moisture transport due to the southerly surge appears to be linked to precipitation along the west coast of the southern Indo-China Peninsula. A case study of the southerly surge event during August 2000 illustrates the formation of the equatorial clockwise gyre and its convectively coupled equatorial Rossby wave signature.

Citation: Fukutomi, Y., and T. Yasunari (2009), Cross-equatorial influences of submonthly scale southerly surges over the eastern Indian Ocean during Southern Hemisphere winter, *J. Geophys. Res., 114,* D20119, doi:10.1029/2008JD011441.

1. Introduction

[2] Lower-tropospheric southerly wind surges from the extratropics into the tropics regulate the tropical convective activity over the eastern Indian Ocean (EIO) during Southern Hemisphere (SH) winter [*Fukutomi and Yasunari*, 2005, hereafter referred to as FY05]. FY05 reported strong evidence that the submonthly (6–25 days) southerly surges are extratropical-tropical interaction phenomena that involve a variety of processes, such as development of tropical convection, dry and cold air advection from the extratropics into the tropics, and air-sea interaction in the EIO region. The southerly surges are caused by midlatitude Rossby wave propagation from the southwestern Indian Ocean through the South Pacific. The strong baroclinic development of Rossby waves in the entrance region of the SH wintertime subtropical westerly jet off the west coast of Australia amplifies the low-level southerlies, leading to the southerly surges over the EIO.

[3] FY05 concentrated on the impacts of the southerly surges on tropical convection. They mainly discussed the physical processes associated with the local blowup of convection that subsequently occurs after the surge peak. Interestingly, they also noticed a cross-equatorial connection between southerly surges and the South Asian monsoonal circulation and convection. Southerly surge enters the southern Bay of Bengal (BOB), forming transient cross-equatorial flow that encompasses the whole tropical EIO region. The cross-equatorial flow turns clockwise and

[1]Frontier Research Center for Global Change, Japan Agency for Marine-Earth Science and Technology, Yokohama, Japan.
[2]Hydrospheric Atmospheric Research Center, Nagoya University, Nagoya, Japan.

0148-0227/09/2008JD011441$09.00

merges into the monsoon westerly flow over South Asia around 5° to 10°N. Coherent strengthening of an equatorial clockwise gyre and westerly winds with the surge event are seen over the southern Bay of Bengal. The surge-induced cross-equatorial flow appears to produce the equatorial wave disturbance. Nevertheless, the underling physical processes for the dynamical impacts exerted by the southerly surges have not been well discussed.

[4] Many previous works have recognized that transient cross-equatorial flows associated with meridional wind surges exert important lateral forcing on tropical disturbances such as westerly wind bursts, convectively coupled equatorial waves, and tropical cyclones in the broad Indian Ocean-Pacific region. For example, northerly cold surges from the East Asian extratropics and their related cross-equatorial flows play a role in the development of equatorial westerly wind bursts in the western Pacific [e.g., *Murakami and Sumi*, 1981; *Love*, 1985a, 1985b; *Chu*, 1988; *Sumathipala and Murakami*, 1988; *Chu and Frederick*, 1990; *Kiladis et al.*, 1994; *Meehl et al.*, 1996; *Suppiah and Wu*, 1998; *Yu and Rienecker*, 1998; *Compo et al.*, 1999; *Yu et al.*, 2003]. In addition, the northerly surges have effects on tropical cyclones and other near-equatorial vortex-type disturbances over the Maritime Continent [e.g., *Love*, 1985b; *Chang et al.*, 2003, 2005]. As documented by FY05, southerly surges on various timescales and their related cross-equatorial flows originating in the Southern Hemisphere extratropics are able to induce equatorial westerly wind events [e.g., *Wang and Murakami*, 1987; *Shrestha and Murakami*, 1988; *Murakami*, 1988; *Murakami and Sumathipala*, 1989; *Hartten*, 1996; *Straub and Kiladis*, 2003]. There is also evidence that tropical cyclogenesis is influenced by cross-equatorial flow from the SH [e.g., *Love*, 1985a, 1985b].

[5] Several of the above studies discussed the generation mechanisms of equatorial westerly wind events that are preceded by the meridional wind surge; specifically, equatorward propagation of surface high-pressure perturbation (i.e., pressure surge) accompanied by the meridional wind surge enhances the zonal (west-east) pressure gradient around the equator, which then sets up strong westerly wind events [*Love*, 1985a; *Chu*, 1988; *Chu and Frederick*, 1990; *Yu et al.*, 2003]. In addition, equatorial zonal wind events are formed as a part of equatorially trapped Rossby or Kelvin waves excited by the meridional wind surges [e.g., *Kiladis et al.*, 1994; *Straub and Kiladis*, 2003]. On the basis of numerical simulation results, *Lim and Chang* [1981] and *Zhang and Webster* [1992] gave a theoretical basis for equatorial waves forced by cross-equatorial surge flows that was similar to those observed by the above studies.

[6] Our current concern is the fundamental mechanism that drives the equatorial wave disturbances following the southerly surges over the EIO. As mentioned above, spatially and temporally coherent structures in low-level circulation on the NH side of the EIO-southern Bay of Bengal region were observed during the surge event. The purpose of this study is to confirm that the southerly surges are the forcing for the equatorial disturbances and to explore how the surge-induced cross-equatorial flows force the equatorial disturbances. We attempt to determine the role of the southerly surge in the creation of the clockwise equatorial gyre. We first reconfirm the cross-equatorial teleconnective nature of the surge by composite analysis of atmospheric fields. We then analyze the impacts of the cross-equatorial flow using dynamical diagnostics. This paper is organized as follows: section 2 briefly describes the data and analysis procedure used. Basic structures of the surge-related atmospheric fields are discussed in section 3. Results from dynamical analysis, conducted to ensure the cross-equatorial effects of the surge, are presented in section 4. Section 5 describes regional hydrological impacts, while section 6 analyzes a case of surge-induced equatorial disturbance. Finally, section 7 presents a summary and discussion.

2. Data and Methods

[7] For this study, we used a global atmospheric reanalysis data set and a satellite-based precipitation data set. The atmospheric reanalysis data set is the Japanese 25-Year Reanalysis (JRA25), which covers the period from 1979 through 2004. This data set was recently produced by the Japan Meteorological Agency (JMA) numerical assimilation and forecast system and provides many kinds of assimilated and forecasted variables available at a 6-hour temporal resolution and various grid types [*Onogi et al.*, 2005, 2007]. We used the atmospheric horizontal winds, geopotential height, temperature, and specific humidity on horizontal 2.5° grids and 12 pressure levels (1000, 925, 850, 700, 600, 500, 400, 300, 250, 200, 150, and 100) from the ganl-p25h subset of JRA25 [see *Onogi et al.*, 2007]. Following the method of FY05, we computed stream function, velocity potential, divergence, vorticity, and divergent winds from horizontal winds using a spherical harmonic transform method. All the atmospheric variables were daily averaged before data analysis.

[8] The precipitation data set is the Tropical Rainfall Measuring Mission satellite (TRMM) 3B42 product [*Kummerow et al.*, 2000] obtained from the National Aeronautics and Space Administration (NASA)/Goddard Space Flight Center (GSFC). This data set covers the period from 1998 through the present on a 0.25° spatial and with a 3-hour temporal resolution. The precipitation data were regridded on a 1° grid by spatial averaging and then daily averaged.

[9] The data analysis was carried out during June-July-August (JJA) for a 7-year period from 1998 to 2004 when both JRA25 and TRMM data are commonly available. Most of the data processing and analysis methods employed here are similar to those used in our previous study (FY05). Anomaly time series of all variables were computed by removing the first three harmonics from the original 365-day time series. The anomaly time series were then filtered into a 6- to 25-day band using a Butterworth filter [*Kaylor*, 1977]. To establish the relationships between the low-level southerly surges and large-scale dynamical fields, we began by identifying the southerly surge events using the same procedure as FY05. The selection of cases was based on the surge index. The index was defined during JJA of each year by the area-averaged 850-hPa meridional wind time series over the box (87.5–92.5°E, 17.5–2.5°S). This grid box encloses the region of maximum variance of the 6- to 25-day filtered 850-hPa meridional

wind in the tropics of the EIO (see FY05). The surge events were defined by strong positive peaks of this index, with values exceeding the criterion of climatological 1.5 standard deviation (2.2 m s^{-1}). In total, 21 surge events were found during the seven JJA seasons. These events (surge peak phases) are referred to as the key dates for compositing. Daily lag composites of various fields were constructed relative to these key dates, denoted by day 0 phases.

[10] It should be noted here that we confirmed enhanced activity of submonthly disturbances over the EIO prior to the composite analysis. We compared several statistical characteristics obtained from JRA25 with those shown by FY05 (not shown). A spatial pattern of variance of the 6- to 25-day filtered 850-hPa meridional wind was similar to that in the FY05 results. A variance maximum over the EIO was observed also in the present results. In addition, power spectra of unfiltered anomalous time series of the 850-hPa meridional wind in the box defined for the surge index had dominant power in the submonthly range. Hence these results must justify our choice of a frequency range for time filtering.

3. Development of Equatorial Waves Associated With the Southerly Surge

3.1. Basic Circulation Patterns

[11] This section examines the space-time evolution of low-level circulation anomalies in the Indian Ocean-south Asian region. Composite maps were created from the 21 surge events to highlight the development of the equatorial wave disturbance that might be induced as a response to the southerly surge. Figure 1 shows a composite sequence of 850-hPa winds. The most important feature is the evolution of the equatorial clockwise gyre just after cross-equatorial penetration of the southerly surge.

[12] From days −2 through 0, the pathway of the southerly surge is well established. Southerly-southeasterly wind anomalies cross the equator and reach the southern Bay of Bengal. At day 0, the cross-equatorial southerly flow turns clockwise and merges with the westerly flow over the southern Bay of Bengal-Southeast Asia. This continuous flow forms an anticyclonic circulation (clockwise gyre: cyclonic circulation in the SH side) centered on northwestern Sumatra Island. After the penetration of the southerly flow, this clockwise gyre moves westward along the equator and develops over the equatorial EIO by day +3. The equatorial clockwise gyre is mostly strengthened from day+2 through day +3. Westerlies along the northern flank of the equatorial clockwise gyre are enhanced toward the western Pacific. Simultaneously, an off-equatorial cyclonic circulation (anticlockwise gyre) is also strengthened over the northern Bay of Bengal. After day +3, a pair of north-south gyres moves further westward to the western Indian Ocean-Arabian Sea region with slight decaying. The north-south double gyre structure during the period from day +1 through day +5 is very similar to that of the 10- to 20-day monsoon mode [e.g., *Chen and Chen*, 1993; *Goswami and Ajaya Mohan*, 2001]. As pointed out also by FY05, the excitation of the equatorial clockwise gyre could be a result of the southerly surge. This clockwise gyre is interpreted as a kind of equatorially trapped Rossby wave, which is asymmetric about the equator [e.g., *Chatterjee and Goswami*, 2004] and a response to the surge-induced cross-equatorial flow.

3.2. Vorticity and Divergence Anomalies

[13] To trace clearer and sharper structures of the equatorial clockwise gyre, a composite sequence of relative vorticity anomalies is displayed in Figure 2 together with divergence anomalies. The region of negative vorticity anomalies (Figures 2a–2d) corresponding to the equatorial clockwise gyre (Figure 1) extends southeastward from northwest of the islands of Sumatra into the equatorial central Indian Ocean. Initially, an anticyclonic (clockwise) vortex center is formed east of the Sumatra islands near 5°N, 92.5°E at the surge peak phase (Figure 2a). The vortex center subsequently moves southwestward and crosses the equator, and then arrives at 2.5°S, 80°E by day +3. At the same time, the negative anomalies form a zonally elongated band. Note that the region of negative vorticity anomalies is equivalent to that of anomalous cyclonic shear on the SH side.

[14] Convergent anomalies (Figures 2e–2f) also develop along 5°S just after the surge peak phase. Weak convergent regions have already appeared south of the equator at day 0. On the other hand, divergent anomalies prevail in the off-equatorial surge region, which reflects a divergent characteristic of the southerly surge flow. A zonally elongated convergent band grows from day +1 through day +2 along the SH side equatorial zone spanning 5°S–0. The low-level convergence following the surge peak can be caused by a boundary layer frictional effect on the surge flow as discussed by FY05. The convergent band is aligned with the anomalous negative (cyclonic) vorticity band (Figures 2a–2d) during the period from day +1 through day +3. In addition, the convergent band appears to lead the evolution of the negative vorticity band south of the equator. This implies that the surge-induced convergence may contribute to generating the cyclonic shear as a part of the clockwise gyre through a vortex stretching effect. That matter is discussed in section 4.

3.3. Vertical Structure

[15] To examine the vertical structure of the equatorial clockwise gyre, longitude-height cross sections of composite relative vorticity anomalies averaged around the equator (2.5°S–2.5°N) from day +1 to day +4 are displayed in Figure 3. This 4-day period includes the development and mature stages of the gyre. On day +1, a region of negative anomaly extends from the lower troposphere to the upper troposphere between 80° and 100°E, suggesting a deep equivalent barotropic structure of the gyre throughout the troposphere. After day +2, a core of negative anomaly shifts westward, and a region of positive anomaly appears in the upper troposphere. From day +3 to day +4, the vertical structure exhibits a first baroclinic structure throughout the troposphere between 60° and 90°E. The equivalent barotropic structure with negative anomalies is still pronounced in the lower and middle troposphere up to roughly 400 hPa. On the other hand, a positive anomaly aloft at about 100–300 hPa is quite obvious. This baroclinic structure is likely caused by the convective development 2–4 days after the surge peak as shown by FY05 (in their Figure 4) and Figure 8 in the later section.

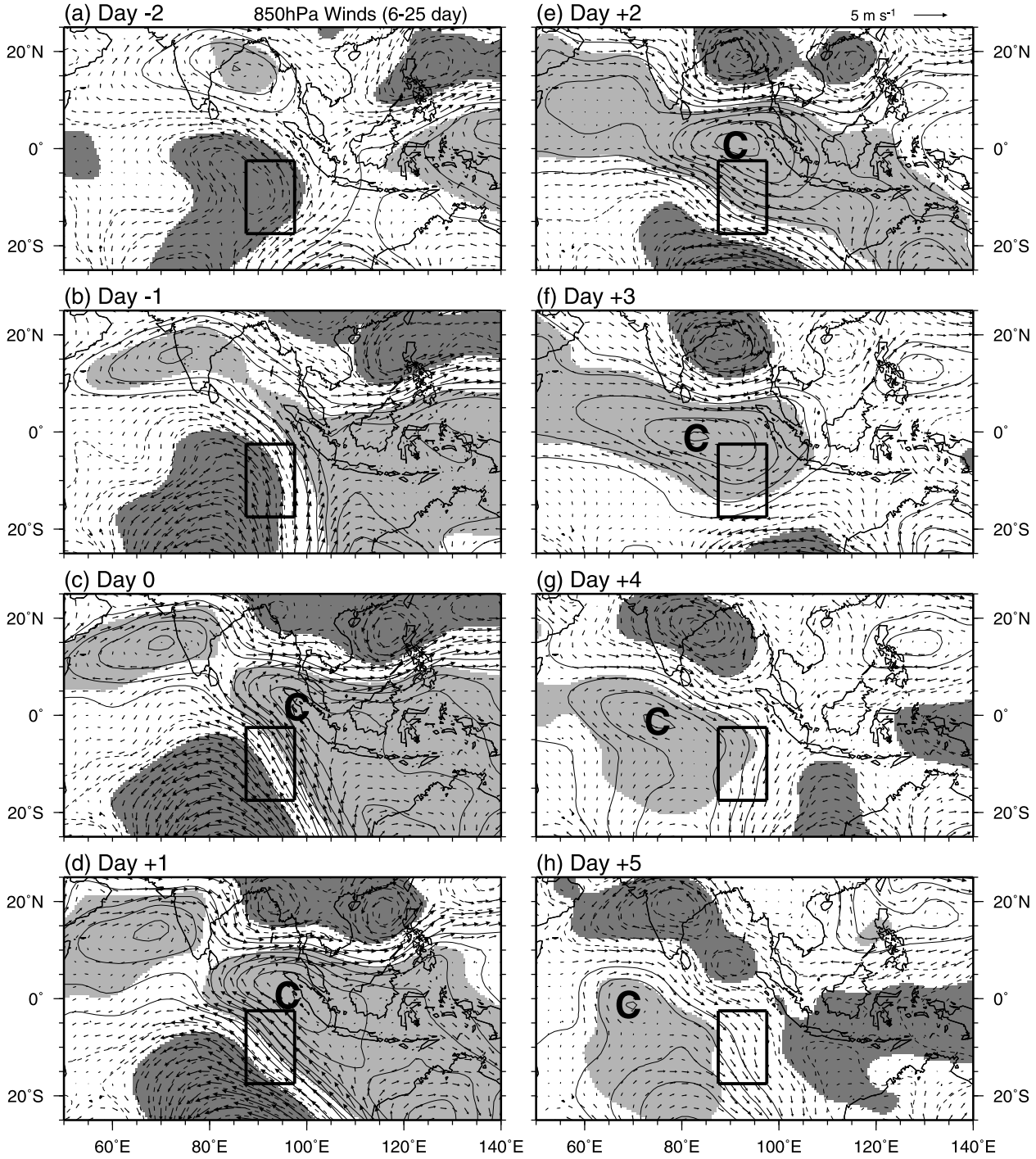

Figure 1. Composites of 6- to 25-day filtered 850-hPa wind vector anomalies and stream function anomalies (contours) from day −2 through day +5 with 1-day interval based on the surge index. Solid (dashed) contours are positive (negative) values. Contour interval is 4.0×10^5 m^2 s^{-1}. Zero contours are omitted. Light (dark) shading indicates the positive (negative) stream function anomalies at the 95% level. gCh represents the center of the equatorial clockwise gyre.

3.4. Westward Propagating Wave Characteristics

[16] As aforementioned, the equatorial clockwise gyre is presumably consistent with an equatorial Rossby wave-type disturbance. To obtain insight into equatorial Rossby wave characteristics of the gyre, a longitude-time cross section of composite relative vorticity anomalies along the equator (2.5°S–2.5°N) in the Indian Ocean region is illustrated in Figure. 4. The clear westward phase propagation of negative anomalies is evident after the surge peak phase (day 0). A core of the negative anomalies which corresponds to the center of the equatorial clockwise gyre is formed by day +2. Then, these anomalies propagates westward by roughly

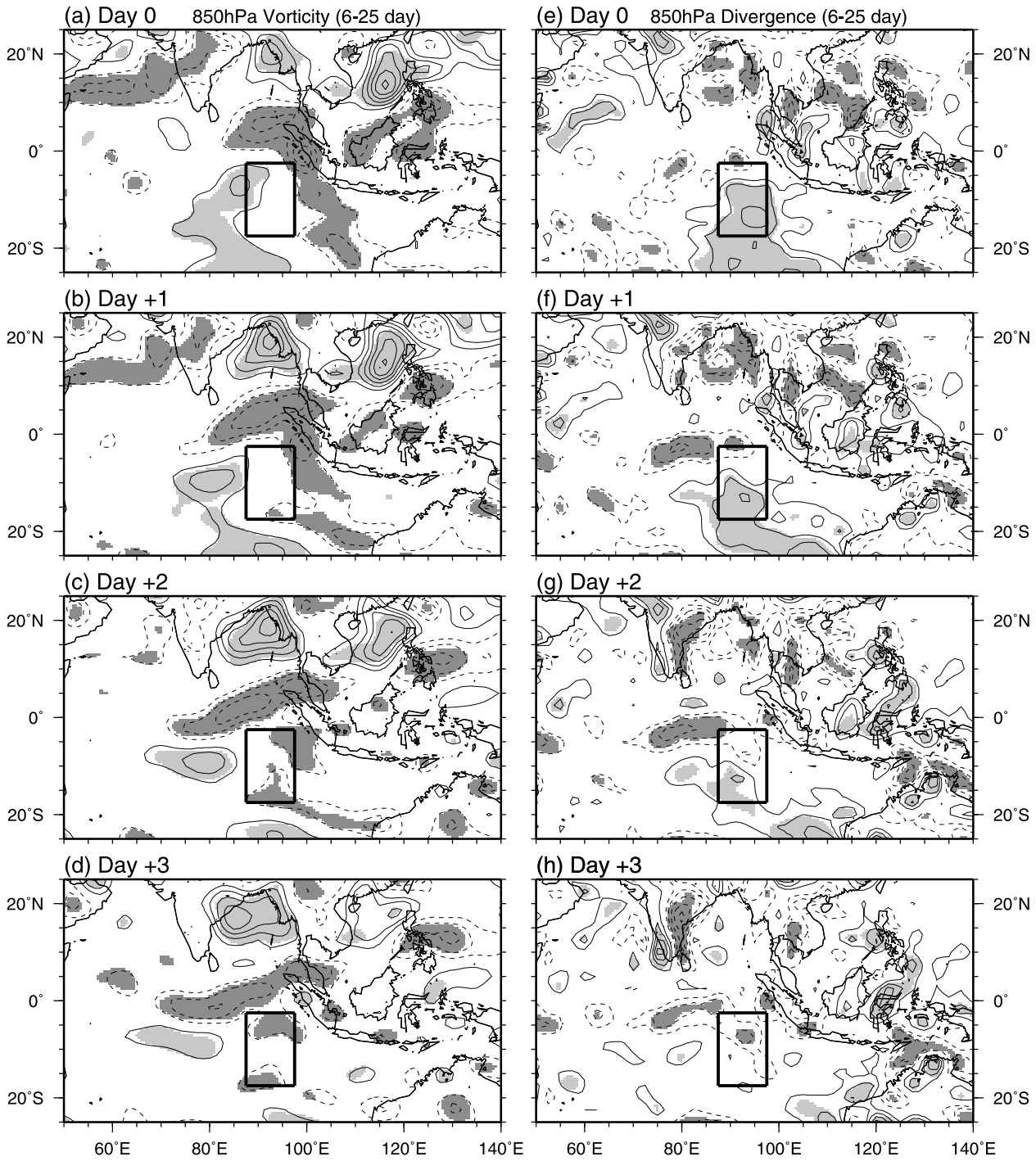

Figure 2. Composites of 6- to 25-day filtered 850-hPa (a, b, c, and d: left) relative vorticity anomalies and (e, f, g, and h: right) divergence anomalies from day 0 through day +3. Solid (dashed) contours are positive (negative) values. Contour interval of the relative vorticity (divergence) anomalies is 2.0×10^{-6} s^{-1} (0.5×10^{-6} s^{-1}). Zero contours are omitted. Light (dark) shading indicates positive (negative) anomalies significant at the 95% level.

day +7. The westward phase speed estimated from this plot is approximately 7 m s^{-1}. This value is somewhat greater than the phase speeds estimated by previous works on the equatorial Rossby waves in the tropical Indian Ocean–South Asian Monsoon region [e.g., *Chatterjee and Goswami*, 2004; *Yokoi and Satomura*, 2005]. However, our estimate is adequately within the range of typical phase speed of equatorial Rossby waves identified by several studies [e.g., *Kiladis and Wheeler*, 1995; *Pires et al.*, 1997]. We measured also the size of the gyre along the equator by the relative vorticity composites (Figures 2, 3, and 4). The zonal scale of the gyre is estimated to be 3000–4000 km

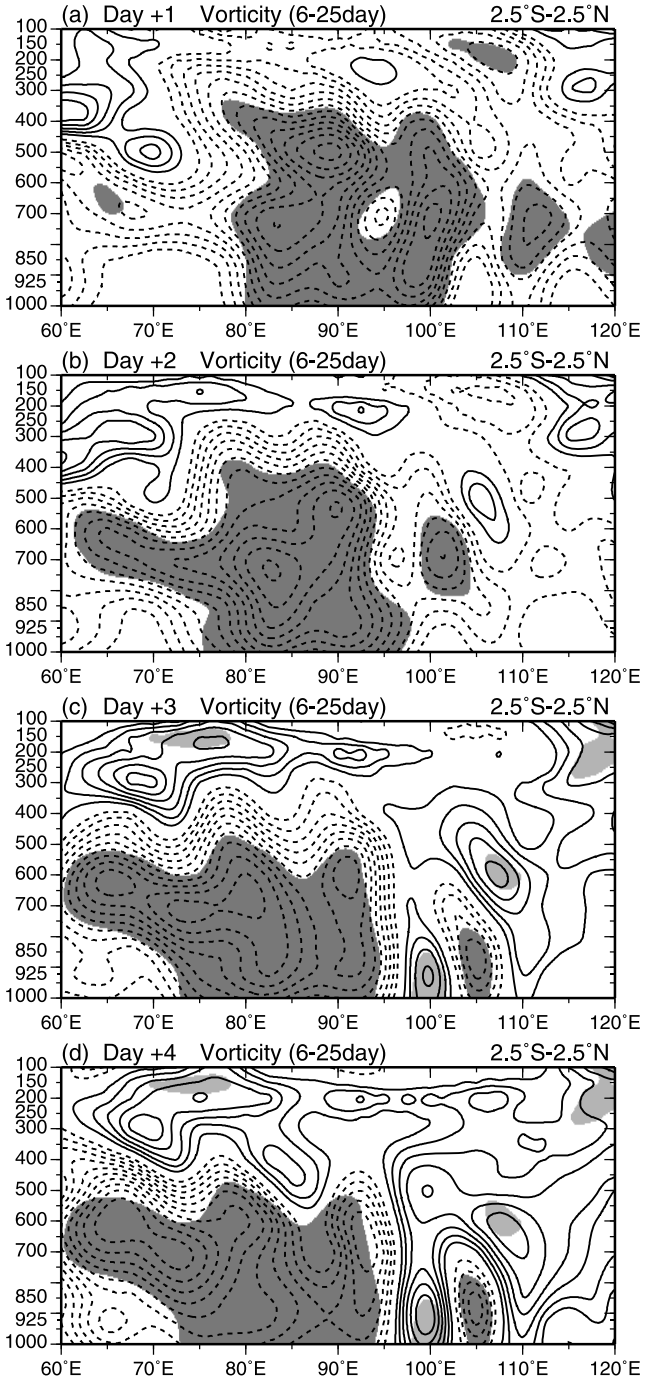

Figure 3. Longitude-height cross sections of composite of 6- to 25-day filtered relative vorticity anomalies along 2.5°S–2.5°N from day +1 through day +4. Contour interval is 0.5×10^{-6} s^{-1}. Zero contours are omitted. Light (dark) shading indicates positive (negative) anomalies significant at the 95% level.

which can be equivalent to a half wavelength of a wave including the gyre. Therefore we estimate wavelengths of 6000–8000 km (zonal wave numbers 5–7). These values are close to the wavelengths estimated by the previous studies. Overall, these space-time characteristics suggest that the equatorial clockwise gyre identified in the present analysis could be interpreted as an equatorial Rossby wave.

4. Dynamical Diagnostics for the Equatorial Wave Genesis

4.1. Vorticity Budget Analysis

[17] The composite sequences (Figures 1 and 2) above reveal the formation and movement of the equatorial clockwise gyre. Transient negative vorticity accumulation in the equatorial EIO region might create the clockwise gyre following the surge event. It is interesting that the clockwise gyre begins to develop mainly from the NH side (Figure 2a) in conjunction with the anticyclonic turning of the surge-induced cross-equatorial flow (Figure 1). One can thus expect that this transient cross-equatorial flow advects negative vorticity from the SH into the NH side of the equatorial region, which would play a vital role in the increase of negative eddy vorticity in the region. To understand the physical processes responsible for the growth of the equatorial clockwise gyre, we employ vorticity budget analysis. The equation governing transient eddy vorticity tendency can be derived as

$$\frac{\partial \zeta'}{\partial t} = \underbrace{-\mathbf{V}' \cdot \nabla(\overline{\zeta}+f)}_{\text{ADV1}} \underbrace{- \overline{\mathbf{V}} \cdot \nabla \zeta'}_{\text{ADV2}} \underbrace{- D'(\overline{\zeta}+f)}_{\text{DIV1}} \underbrace{- \overline{D}\zeta'}_{\text{DIV2}} + R \quad (1)$$

where ζ is the vertical component relative vorticity, t is time, f is the Coriolis parameter, D is the horizontal divergence, $\mathbf{V}$ is the horizontal wind vector, and R is the residual. Primes denote submonthly (6–25 days) eddy components, and overbars refer to low-frequency basic states defined as 25-day low-pass smoothed values.

[18] The first term on the right-hand side is the advection of basic state absolute vorticity by submonthly eddy winds (ADV1); the second term is the advection of the submonthly eddy vorticity by the basic state winds (ADV2); the third term is the vortex stretching due to submonthly eddy divergence (DIV1); and the fourth term is the vortex stretching due to the basic state divergence (DIV2). The

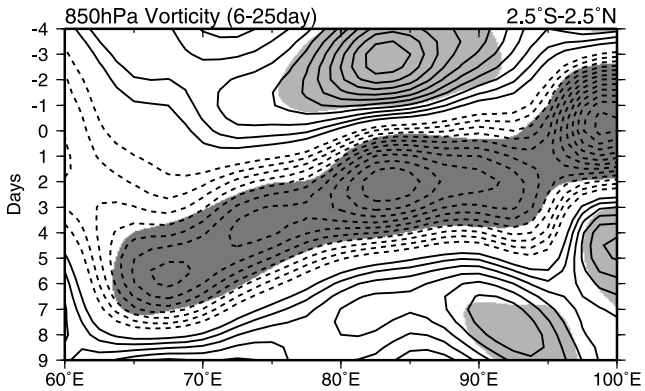

Figure 4. Longitude-time cross section of composite of 6- to 25-day filtered 850-hPa relative vorticity anomalies averaged between 2.5°S and 2.5°N. Contour interval is 0.5×10^{-6} s^{-1}. Zero contours are omitted. Light (dark) shading indicates positive (negative) anomalies significant at the 95% level.

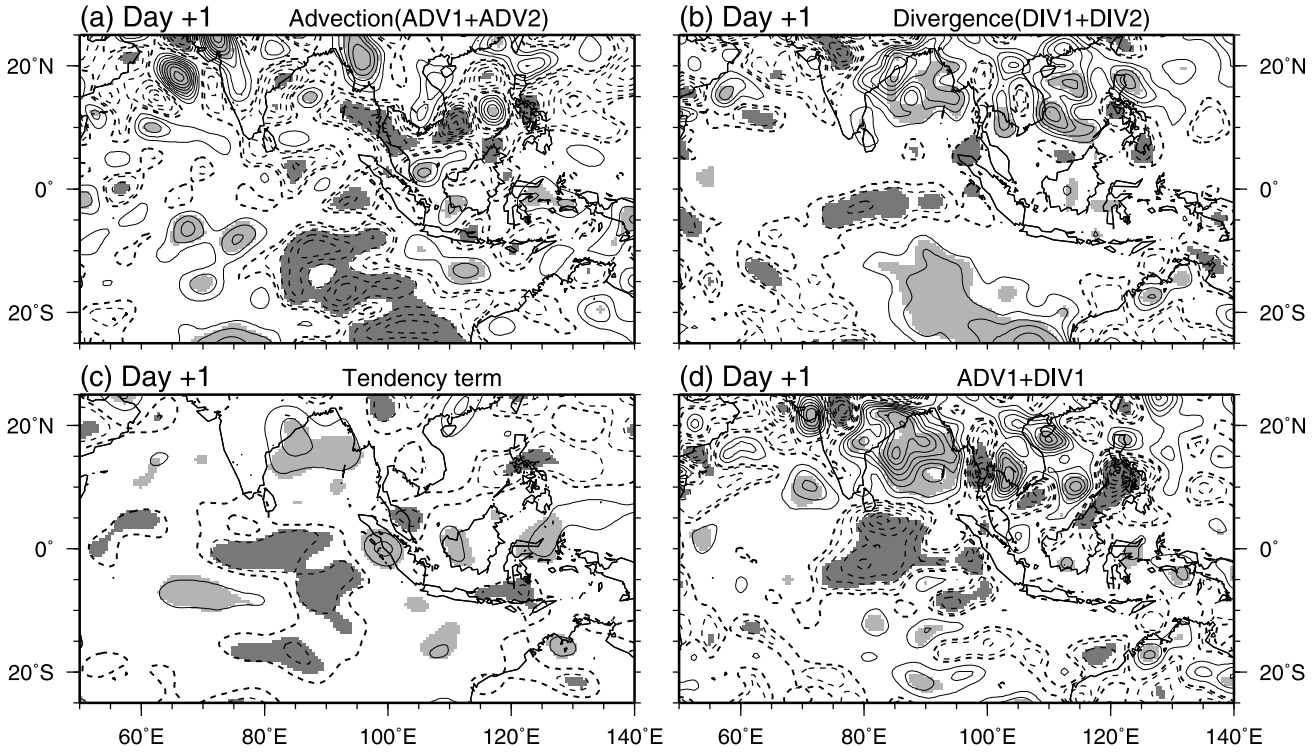

Figure 5. Composites of terms in the eddy vorticity tendency equation at day +1 (see text for details): (a) total advection effect (ADV1 + ADV2), (b) total divergence effect (DIV1 + DIV2), (c) eddy vorticity tendency, and (d) sum of the two terms (ADV1+DIV1) at 850 hPa. Contour intervals are 2.0×10^{-11} s^{-2}. Zero contours are omitted, and −1.0 unit contours are added. Light (dark) shading indicates positive (negative) anomalies significant at the 95% level.

residual term R contains the twisting, vertical advection, and all other terms. This formulation of the vorticity equation is similar to that employed by *Yokoi and Satomura* [2006]. We directly computed the eddy vorticity tendency term on the left and the four primary terms on the right (ADV1, ADV2, DIV1, DIV2), and then used these terms to investigate the effects of surge-induced eddies in the generation of the equatorial clockwise gyre.

[19] Figure 5 displays composite patterns of the computed terms in equation (1) on day +1. This phase corresponds to the development stage of the gyre just after the surge peak, as seen in Figures 1 and 2. We present the total advection effect (Figure 5a: ADV1+ADV2), the total divergence effect (Figure 5b: DIV1+DIV2), the eddy vorticity tendency (Figure 5c), and the sum of ADV1 and DIV1 (Figure 5d).

[20] Off-equatorial negative tendencies south of 5°S over the EIO are dominated by the advection effect (Figure 5a). Generation of cyclonic shear (negative vorticity tendencies) by the advection effect occurs along the surge region. Negative anomalies are also observed near and northwest of Sumatra Island and southeast of Sri Lanka. These near equatorial signals had already been observed on day −1 through day 0 (not shown) and dominated the initial development of the clockwise gyre from day −1 through day +1. It is noteworthy that the distribution of ADV1 (Figure 6d) resembles the distribution of total advection (Figure 5a). In particular, ADV1 indicates larger values around the equator, suggesting the importance of the direct effect of the surge winds. Additionally, ADV2 (not shown) is predominantly positive in the region of ADV1 negative around the equator to the southeast of Sri Lanka. Hence ADV2 works as a dissipater for the negative vorticity in the region. ADV1 and ADV2 compensate each other; however, the absolute magnitude of the negative ADV1 is larger than that of the positive ADV2. As a result, the total advection (ADV1 + ADV2) is still negative in the region, as shown in Figure 5a. In summary, the surge-induced cross-equatorial flow entering the southern Bay of Bengal tends to inject the basic state negative vorticity northward into the NH side, which drives the anticyclonic (negative) vorticity tendency to the north of the equator.

[21] The total divergence effect shapes a zonally elongated narrow band of strong negative values spanning 5°S to 0° (Figure 5b). The band well reflects concurrent negative (cyclonic) tendencies in the same location (Figure 5c). Here the distribution of the DIV1 term (Figure 6h) resembles that of the total divergence effect (Figure 5b). In the region of the negative eddy vorticity tendencies close to the equator (Figure 5c), the magnitude of negative DIV1 values is almost the same degree as that of the negative total divergence effect. Thus the DIV1 term dominates the accumulation of negative eddy vorticity on the SH side equatorial zone, which results in the generation of eddy cyclonic vorticity corresponding to the equatorial gyre. Note that the magnitude of DIV2 was found to be much smaller than that of DIV1 (not shown). DIV2 does not contribute to the negative vorticity increase in this region.

[22] The sum of ADV1 and DIV1 indicates comparatively complex structures (Figure 5d); however, the negative values are concentrated in the region of the negative

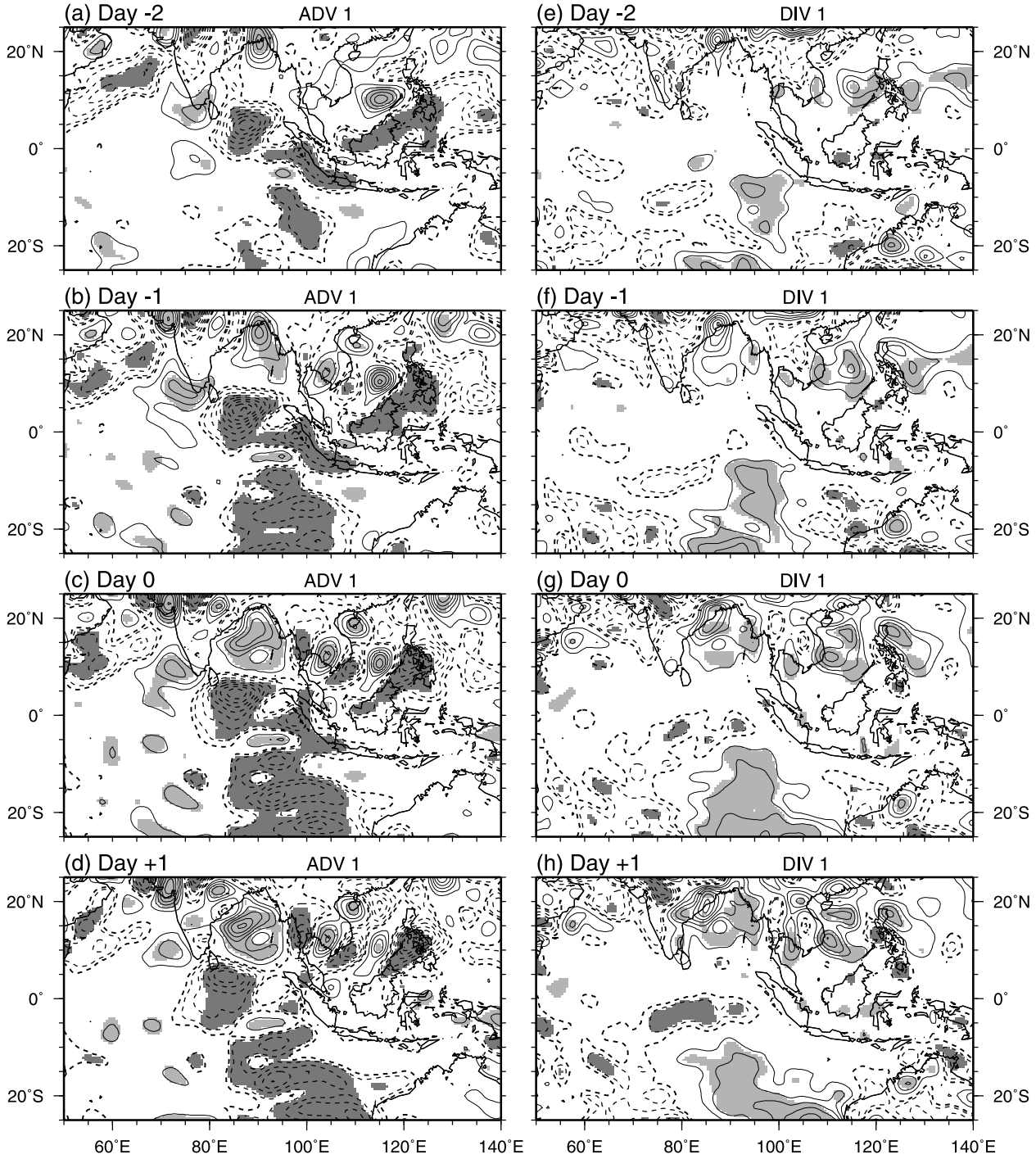

Figure 6. As in Figure 5 for (a–d) ADV1 and (e–h) DIV1 from day −2 to day +1.

tendency around the equator (Figure 5c), emphasizing that combined effects of these terms facilitate the negative eddy vorticity increase in the equatorial EIO. In particular, the southerly surge winds originate in the SH extratropics, and their induced convergence effects (i.e., ADV1 and DIV1) play significant roles in forcing the Rossby wave over the equatorial EIO.

[23] We also computed the vertical advection term, the twisting term, and a nonlinear term defined by eddy vorticity flux divergence included in the *R* term (not shown). The resulting composite distributions of these terms are not well organized, and their magnitudes are quite small compared with the above four terms. Hence the effect of the *R* term can be considered unimportant.

[24] By using the same vorticity budget diagnostics, we additionally document the processes contributing to the maintenance of the off-equatorial cyclonic circulation (anticlockwise gyre) over the Bay of Bengal as seen in the previous section and FY05. The day +1 phase corresponds to the developing stage of the cyclonic circulation because a positive vorticity tendency prevails over the Bay of Bengal (Figure 5c). The sum of terms ADV1 and DIV1 indicates

large positive values over the Bay of Bengal to the north of 10°N (Figure 5d). Besides, ADV1 and DIV1 are predominantly positive in the same region (Figure 6d). These features imply that the positive vorticity tendency is mainly produced by ADV1 and DIV1. However, the total advection (ADV1 + ADV2) is mostly negative over the Bay of Bengal, which is caused by large negative values of ADV2 (not shown). The positive values of ADV1 are substantially canceled by the negative values of ADV2. Consequently, DIV1 can be the most important process that maintains the cyclonic circulation over the Bay of Bengal. It should be noted that the magnitude of DIV2 is rather small and negligible for this discussion.

[25] The contribution of the matured surge flow to the intensification of the equatorial clockwise gyre has been discussed by focusing the stage after the surge peak. Another concern is an initial source of the clockwise gyre which grows as the equatorial clockwise gyre after the surge peak. As has been noted in the previous section, the center of the clockwise gyre already exists in the NH side (near 5°N, 90°E) at day 0 (Figure 2). This gyre moves southwestward and develops along the equator in the later stages (as in Figures 1 and 2). We confirmed that this gyre center is formed by day −1 in the vorticity composites (not shown). In addition, the southerly surge winds begin to blow from day −2 (as in Figure 1 and FY05). The cross-equatorial flow formed by the southerly surge extends to the south of Bay of Bengal at this time. Therefore the developing stage of the southerly surge could be associated with the growth of this initial clockwise gyre in the NH side. A composite sequence of ADV1 (Figures 6a–6d) shows that negative values are collocated with the zone of the southerly surge flow in the EIO region (Figure 1 and FY05). From day −2 through day 0, a region of the negative values is located south of the leading edge of the surge (approximately 5–10°N). This region corresponds to the region of negative vorticity anomalies (i.e. the clockwise gyre) during the same period. These features suggest that ADV1 is an important source of negative vorticity tendency which generates the initial clockwise gyre. The negative values of ADV1 during this period are basically caused by the cross-equatorial southerly surge (eddy) winds. On the other hand, DIV1 (Figures 6e–6h) is not significant in the equatorial EIO region prior to the surge peak. This indicates that the convergent forcing as discussed previously does not work in the developing stage of the surge. Besides, DIV2 is much smaller than other terms and ADV2 is partly offsets ADV1 at the initial clockwise gyre location (not shown). Thus ADV1 is a main contributor to the initial clockwise gyre formation. The advection of basic state absolute vorticity by the southerly surge winds acts to reinforce the initial clockwise gyre prior to the surge peak.

4.2. Wave Activity Flux Analysis

[26] To further emphasize the importance of the lateral forcing due to the southerly surge originating in the SH extratropics, we employed the barotropic version of Plumbfs wave activity flux [*Plumb*, 1986], derived by *Sobel and Bretherton* [1999] and *Sobel and Maloney* [2000]. They successfully diagnosed the low-level Rossby wave energy accumulation over the tropical western Pacific using their wave activity flux definition.

[27] Here the horizontal wave activity flux vector for the transient eddies $\mathbf{M}_T$ consists of the radiative part $\mathbf{M}_R$ and the advective part $\langle \mathbf{V} \rangle M$; that is,

$$\mathbf{M}_T = \mathbf{M}_R + \langle \mathbf{V} \rangle M, \tag{2}$$

where $\langle (\,) \rangle$ is a climatological SH-winter average, and M is the wave activity defined as

$$M = \frac{p\overline{\overline{\zeta'^2}}\cos\phi}{2|\nabla\langle\zeta_a\rangle|} \tag{3}$$

where $\langle \zeta_a \rangle$ is the SH-winter climatology of absolute vorticity, p is pressure normalized by a reference pressure (1000 hPa), and ϕ is latitude. The double overbar indicates a time average over a specific period.

[28] The radiative part is equivalent to the barotropic part of the localized E-P flux of *Trenberth* [1986], except for the pressure factor, which is written as

$$\mathbf{M}_R = p\cos\phi\left[\frac{1}{2}(\overline{\overline{v'^2 - u'^2}}), -\overline{\overline{u'v'}}\right]. \tag{4}$$

[29] The $\mathbf{M}_T$ vectors are parallel to the total group velocity of Rossby wave energy propagation, and the $\mathbf{M}_R$ vectors are parallel to the group velocity relative to the basic state flow. In general, the convergence of $\mathbf{M}_T$ is a good measure of Rossby wave energy accumulation [e.g., *Sobel and Bretherton*, 1999; *Sobel and Maloney*, 2000].

[30] We examined both $\mathbf{M}_T$ and $\mathbf{M}_R$ during the surge period. The transient eddy components of these were estimated from composite submonthly eddy zonal (u) and meridional (v) winds, and relative vorticity. Figure 7 displays the $\mathbf{M}_T$ and $\mathbf{M}_R$ vectors together with their divergence averaged over the period from day −5 through day +5. This period includes the development, mature, and decay stages of the southerly surge event.

[31] The $\mathbf{M}_T$ vectors (Figure 7a) are directed northward–northwestward with their divergent features extending from the subtropical to tropical EIO. A location of these strong fluxes coincides with that of the southerly surge winds (Figure 1). These fluxes substantially originated over the midlatitude EIO at 30° to 40°S (not shown). Interestingly, most of the fluxes to the east of 80°E cross the equator and reach approximately 5°N. Therefore it is reasonable to suppose that northward propagation of Rossby wave energy from the SH midlatitudes into the NH equatorial region occurs along the southerly surge flow. Areas of the northward wave activity flux convergence occur around the equator. In comparison with the vorticity anomaly composites (Figure 2), these convergence spots are collocated with the region of negative vorticity anomalies corresponding to the equatorial gyre. This implies that the wave activity flux and its convergence associated with the southerly surge lead to the growth of the equatorial gyre as a part of tropical Rossby waves.

[32] The $\mathbf{M}_R$ vectors (Figure 7b) are used as a measure of eddy activity and their propagation characteristics during the surge period. Similar to $\mathbf{M}_T$ (Figure 7a), a northward component of the radiative fluxes is enhanced in the surge region. The angle of $\mathbf{M}_R$ vectors is somewhat different from

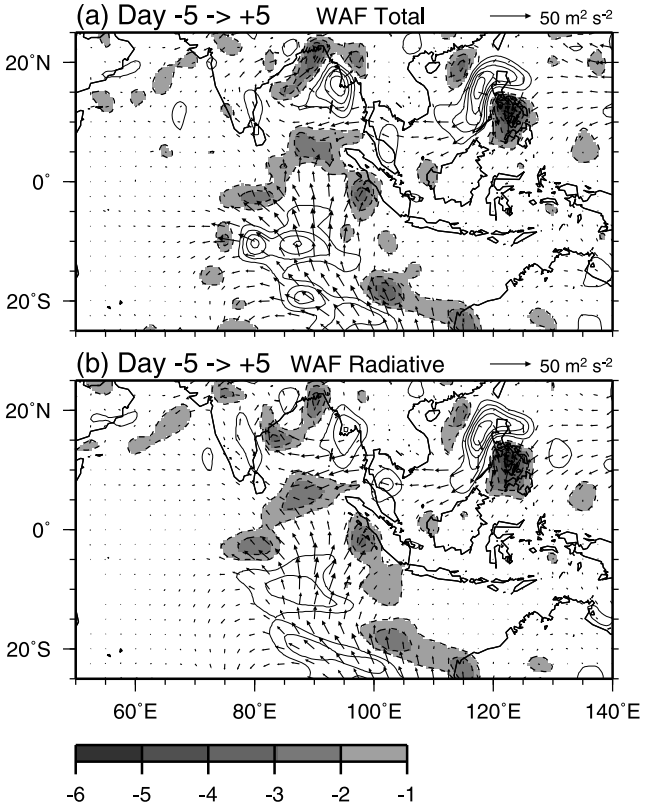

Figure 7. (a) Wave activity flux $\mathbf{M}_T$ and its divergence averaged over day −5 to day +5. (b) As in Figure 7a, except for radiative component $\mathbf{M}_R$ of $\mathbf{M}_T$. The unit of the wave activity flux is $m^2\ s^{-2}$. The divergence (convergence) is represented by solid (dashed) contours with $1.0 \times 10^{-6}\ m\ s^{-2}$ interval. Zero contours are omitted. Areas of the convergence less than $-1.0 \times 10^{-6}\ m\ s^{-2}$ are shaded.

that of $\mathbf{M}_T$ vectors; however, their magnitudes are very similar, suggesting that the contribution of the radiative part to the total wave activity flux is significantly large. In other words, the northward component of the $\mathbf{M}_T$ vector is dominated by the radiative flux $\mathbf{M}_R$ over the EIO. This fact supports the idea that the enhanced eddy activity associated with the southerly surge is responsible for the lateral forcing as a form of Rossby wave energy propagation.

5. Hydrological Impacts of the Surge

[33] Next we consider the atmospheric hydrological signatures that are enhanced by the southerly surge. FY05 reported evidence that the convection develops over the SH side of the tropical EIO a few days later than the surge peak. However, they gave only a limited description of the cross-equatorial hydrological impacts. Here we focus on aspects of the NH side precipitation increase following the surge event. Figure 8 gives composite maps of precipitation and vertically integrated moisture flux anomalies. The overall pattern of the moisture flux anomalies is basically similar to that of the low-level wind anomalies (Figure 1). A clear pathway of cross-equatorial moisture transport is created across the EIO-southern Bay of Bengal region around the surge peak (day −1 through day +1). This moisture flow obviously corresponds to the surge-induced cross-equatorial flow. The southerly moisture flow curves clockwise into westerly moisture flow over the southern Bay of Bengal-Andaman Sea region. This westerly moisture flow bursts toward the southern Indo-China Peninsula and the Malay Peninsula (south of 15°N). These features suggest that the surge-induced cross-equatorial flow plays a role in entraining moisture from the SH into the Bay of Bengal and Southeast Asian regions.

[34] Another interesting feature is that a localized positive precipitation anomaly region appears to the west of the southern Indo-China Peninsula in association with the westerly moisture flow burst during day 0 through day +1. We also examined a composite distribution of the moisture flux convergence anomalies (not shown) and confirmed the moisture flow converge in this increased precipitation signal. This increased precipitation signal might be attributable to the transient moisture flow enhanced by the surge.

[35] We turn now to the behavior of the westward-moving equatorial clockwise gyre that was also identified in the composite moisture flux anomalies. This moisture flux gyre is apparently identical to the equatorial clockwise gyre seen in Figure 1. A region of positive precipitation anomalies expands over the EIO during the gyre development, which can be regarded as the convection organization triggered by the surge [FY05]. This region of increased precipitation is accompanied by the low-level convergence band (Figure 2). A clear structure of a convectively coupled equatorial Rossby wave is formed by day +3. The increased precipitation region is well embedded in the gyre at day +3. However, the structure is short lived and not maintained after day +4. In the following days, the gyre moves westward into the central-western Indian Ocean; nevertheless, the region of strong positive precipitation anomalies is not trailed by the gyre. The strong positive precipitation anomalies develop rather eastward within 80° to 100°E as the gyre moves westward. The gyre and the region of strong positive precipitation anomalies (i.e., the convective region) appear to decouple after day +4.

6. August 2000 Case Study

[36] This section presents a typical case of the equatorial wave development following the surge event during early August 2000. The case illustrates the features in the previous composite analysis results. Figure 9 shows submonthly filtered anomalies of 850-hPa winds together with raw precipitation during the period 4–10 August 2000 with 2-day intervals. Note that the southerly surge peak occurs on 6 August. Two days prior to the surge peak (4 August), a comparatively weaker counterclockwise gyre is centered on the equator to the south of Sri Lanka. At the surge peak (6 August), strong cross-equatorial flow penetrates from the SH extratropics into the NH tropics over the EIO. A clockwise (anticyclonic) gyre begins to develop to the northwest of Sumatra. Two precipitation maxima appear along the busting westerly flow at the northern flank of the gyre and along the southeasterly surge flow over the equatorial EIO. Two days later (8 August), the equatorial clockwise gyre moves southwestward with marked intensification. A region of enhanced precipitation expands within the gyre. In particular, the equatorial EIO precipitation

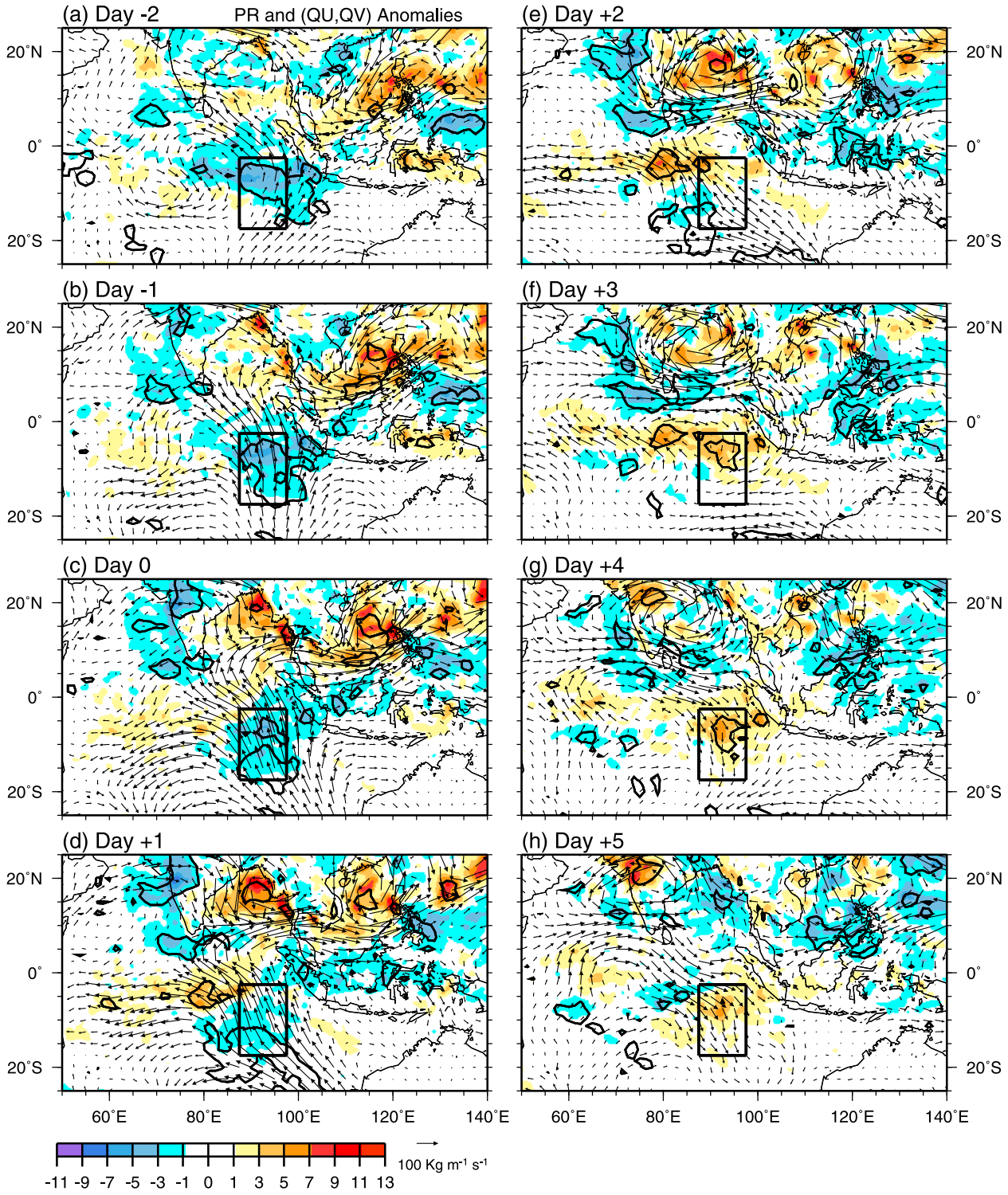

Figure 8. Composites of moisture flux vector (kg m^{-1} s^{-1}) and precipitation (mm day^{-1}) anomalies from day −2 through day +5. The precipitation anomalies are shaded (see color scale bar). Regions enclosed by black contours indicate significant anomalies at 95% level.

increases along the southern flank of the gyre. A convectively coupled equatorial Rossby wave signature is clearly evident at this time. Four days after the surge peak (10 August), the gyre moves westward into the central Indian Ocean. On the other hand, the enhanced precipitation band still remains over the EIO, although it slightly extends toward the central Indian Ocean. The gyre does not trail the precipitation band while it is leaving from the EIO. The decoupling of the gyre and the enhanced precipitation (i.e., convection) region, as pointed out in the previous composite results, is clearly observable in this case.

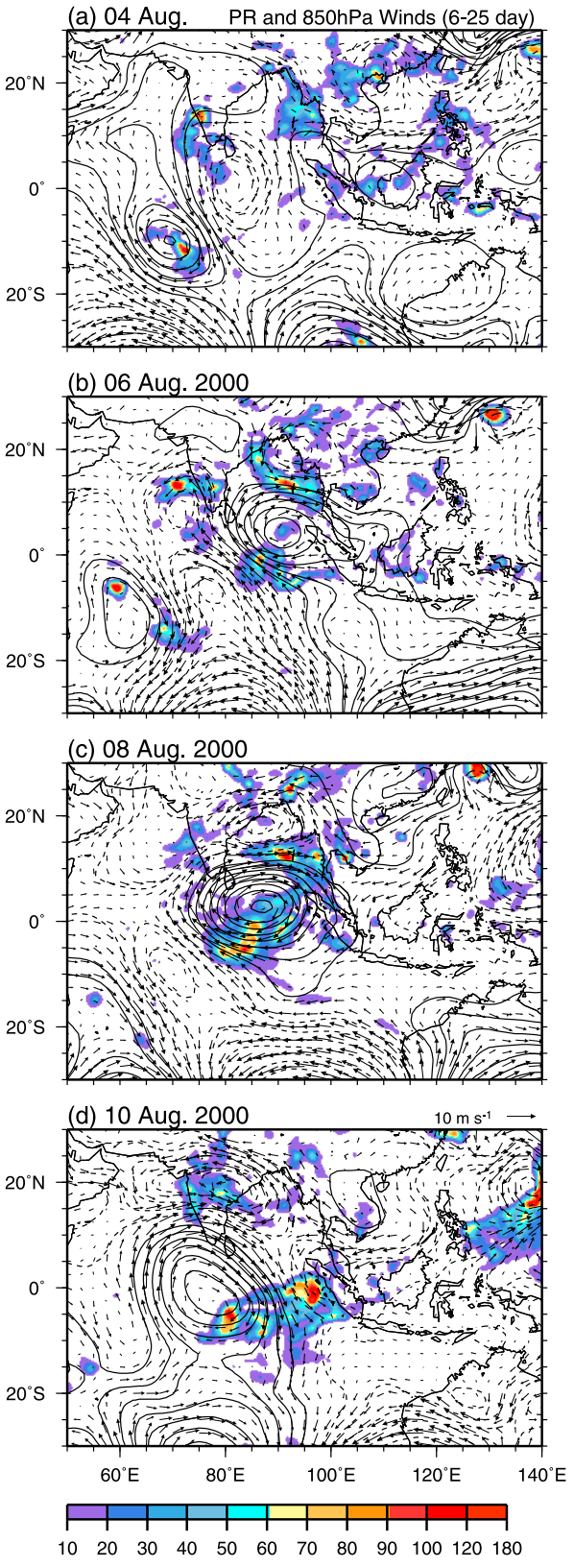

Figure 9. 6- to 25-day filtered wind vector anomalies and stream function anomalies (contours with 1.0×10^6 interval, zero contours are omitted) at 850 hPa and total precipitation (shading) for 4–10 August 2000 with 2-day interval. Precipitation values greater than 10 mm day^{-1} are shaded (see color scale bar).

[37] The structure and evolution of the equatorial clockwise gyre are represented by vorticity fields in Figure 10. The sequence of 850-hPa relative vorticity and wind anomalies (Figures 10a–10d) well captures the growth and westward movement of the gyre associated with the surge-induced cross-equatorial flow. Here a strengthened signature of the equatorial clockwise gyre is also identified in the raw relative vorticity and wind fields (Figures 10e–10h). A westward movement of the center of the gyre can be traced, as seen in the vorticity anomaly fields (Figures 10a–10d). During 6–8 August, the surge-induced cross-equatorial flow is created at the western half of the gyre (75–85°E). A zero absolute vorticity line within this meridian shifts about 5° northward from its position on 4 August, implying the injection of negative absolute vorticity from the SH into the NH due to the cross-equatorial flow.

7. Summary and Discussion

[38] This study examines the cross-equatorial influences of the southerly surges over the eastern Indian Ocean. Emphasis is placed on the dynamical role of the surge-induced cross-equatorial flow in the genesis of the equatorial wave as a form of clockwise gyre. The work was motivated by the fact that low-level meridional surges are an important lateral forcing of tropical disturbances in various locations, especially in the East Asian and western Pacific monsoon regions. We have tried to confirm that this lateral forcing concept is also applicable to the case of the SH winter southerly surge in the eastern Indian Ocean region.

[39] The formation of the equatorial clockwise gyre just after the surge event is well identified in the composites of wind and vorticity anomalies. We interpret this gyre to be a kind of equatorial Rossby wave. To examine a physical mechanism linking the surge and the equatorial clockwise gyre genesis, we conducted eddy vorticity budget analysis. The result suggests the injection of negative absolute vorticity around the equator due to both advective and convergent processes associated with the surge winds. The cross-equatorial advection of the negative basic state absolute vorticity by the surge winds increases negative eddy vorticity in the NH side equatorial region. In addition, the surge-wind convergence accumulates negative eddy vorticity to the south of the equator. The combination of these two processes is primarily responsible for the growth of the equatorial clockwise gyre. Furthermore, the wave activity diagnostics illustrate that the southerly surge that originates in the SH extratropics facilitates northward propagation of Rossby wave energy into the tropics, emphasizing that the southerly surge is an important extratropical forcing of tropical disturbances in the EIO region.

[40] We note not only the dynamical roles but also the hydrological roles of the southerly surge. The cross-equatorial moisture transport caused by the southerly surge appears to partly contribute to the enhancement of precipitation along the west coast of southern Indo-China peninsula. At the peak stage of the equatorial gyre growth, the precipitation maximum is embedded in the gyre, indicating a well-defined convectively coupled equatorial Rossby wave signature. After that, the equatorial gyre moves westward while the precipitation maximum stays over the

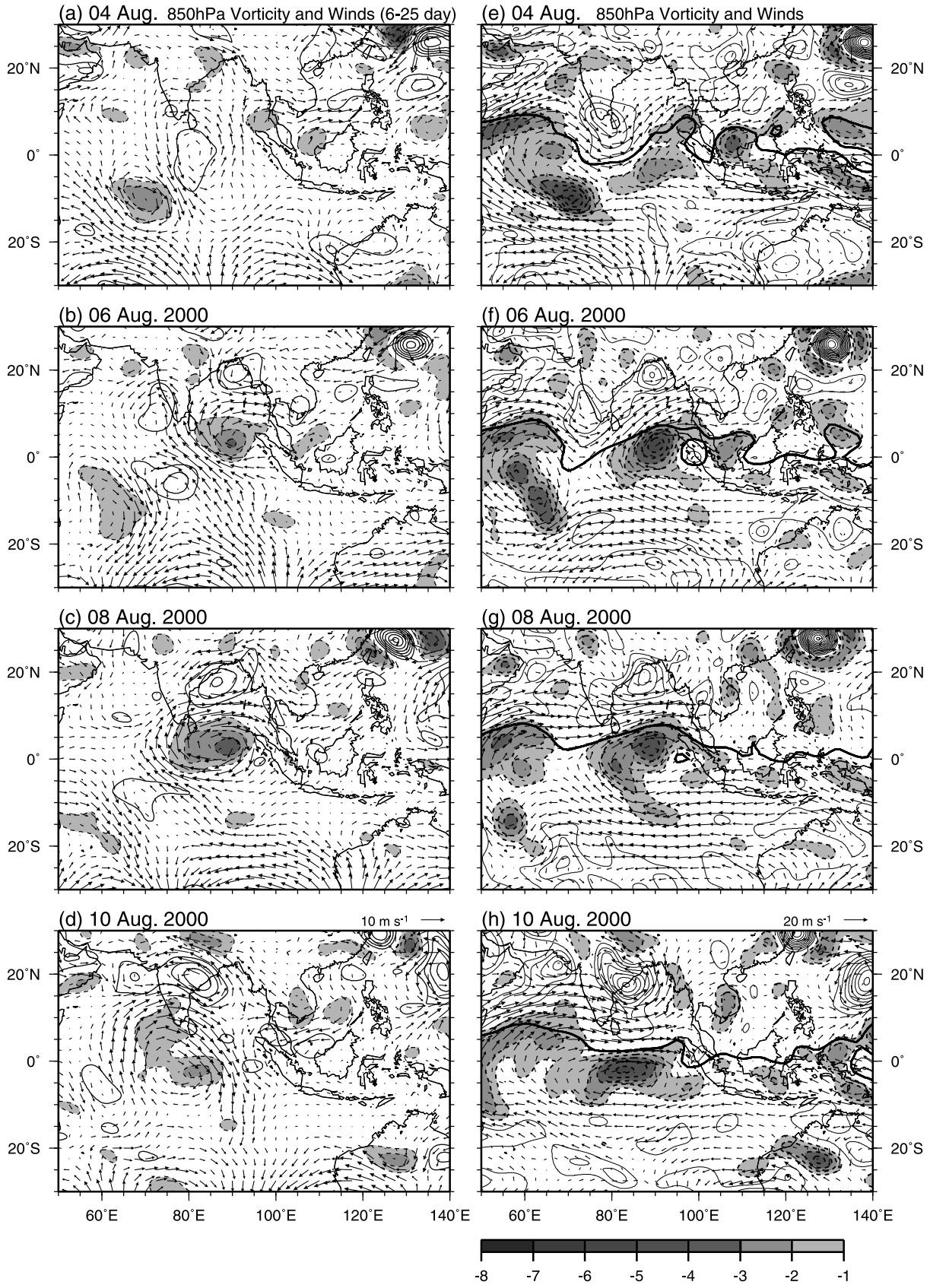

Figure 10. As in Figure 9 except for (a, b, c, and d: left) relative vorticity anomalies and wind vector anomalies and (e, f, g, and h: right) total relative vorticity, total wind vectors, and zero absolute vorticity contour (thick solid line). Contour intervals are 1.0×10^{-5} s^{-1}. Zero contours are omitted. Values less than -1.0×10^{-5} s^{-1} are shaded.

EIO, which suggests the decoupling of the gyre and convection.

[41] The case analysis for August 2000 clearly shows the development of the equatorial clockwise gyre as a convectively coupled equatorial Rossby wave associated with the southerly surge event. Overall features in a sequence of winds, precipitation, and vorticity are almost consistent with those in the composites.

[42] The dynamic structure of the equatorial clockwise gyre that develops after the surge peak accompanies the counterclockwise (cyclonic) gyre over the Bay of Bengal. This north-south double-vortex structure is regarded as an equatorial Rossby wave having an asymmetric pattern with respect to the equator. The pattern is basically similar to an n = 2 equatorial Rossby wave [*Matsuno*, 1966]. However, another possible interpretation for this type of wave pattern has been given by *Chatterjee and Goswami* [2004]. They proposed that this pattern was a translated n = 1 Rossby wave symmetric about the dynamic equator, positioned at approximately 5–10°N. Note that the dynamic equator is defined by the mean absolute vorticity zero line during northern summer [e.g., *Tomas and Webster*, 1997]. Which interpretation is most appropriate is still open to discussion. Further careful investigation is required to compare the observational patterns and the linear theory for equatorial waves.

[43] The transient cross-equatorial flow induced by the southerly surge injects negative absolute vorticity from the SH side into the NH side equatorial EIO region. This process may locally enhance inertial unstable conditions extending from the equator to the dynamic equator [*Tomas and Webster*, 1997], also located in this region. *Tomas and Webster* [1997] pointed out that the Indian Ocean sector during northern summer satisfies the inertial unstable condition as an average feature. They proposed that such a potential condition plays an important role in determining the location of tropical convection in this sector. However, it is unclear whether inertial instability affects the atmospheric conditions disturbed by the submonthly southerly surges examined in the present work. Generally, the timescale of natural oscillation due to inertial instability is approximately 4–5 days around 5°N [*Tomas and Webster*, 1997]. For instance, the absolute vorticity zero line in the case analysis (Figures 10e–10h) migrated northward and southward, in association with the southerly surge and the westward moving equatorial clockwise gyre on a submonthly timescale; however, it did not appear to oscillate over the short period of 4–5 days. It may be difficult to detect the effects of inertial instability on the surge-induced atmospheric conditions because of the dominant submonthly variability in this region.

[44] One of the possible extensions of this study might be an examination of oceanic responses to the submonthly southerly surges. It is important to note that several recent studies have investigated dynamic and thermodynamic responses of the tropical Indian Ocean to atmospheric submonthly variability [e.g., *Sengupta et al.*, 2001, 2004; *Shinoda and Han*, 2005; *Masumoto et al.*, 2005; *Han et al.*, 2006; *Masumoto et al.*, 2008; *Ogata et al.*, 2008]. However, most of these studies have not focused on the ocean circulation and thermal structures that depend on seasonality and the types of atmospheric submonthly disturbances. Future work should take these aspects into consideration.

[45] **Acknowledgments.** We appreciate the comments of three anonymous reviewers, which helped to improve the paper. We thank Bin Wang and Kazuyoshi Kikuchi for providing insightful discussions. This research was initiated while Y.F. was a visiting researcher at International Pacific Research Center (IPRC), University of Hawaii at Manoa from October 2005 through September 2006. This research was supported in part by the JAMSTEC-IPRC joint research program (2005–2006).

References

Chang, C.-P., C.-H. Liu, and H.-C. Kuo (2003), Typhoon Vamei: An equatorial tropical cyclone formation, *Geophys. Res. Lett.*, *30*(3), 1150, doi:10.1029/2002GL016365.

Chang, C.-P., P. A. Harr, and H.-J. Chen (2005), Synoptic disturbances over the equatorial South China Sea and western maritime continent during boreal winter, *Mon. Weather Rev.*, *133*, 1150, 489–583.

Chatterjee, P., and B. N. Goswami (2004), Structure, genesis and scale selection of the tropical quasi-biweekly mode, *Q. J. R. Meteorol. Soc.*, *130*, 1171–1194.

Chen, T.-C., and J.-M. Chen (1993), The 10–20 day mode of the 1979 Indian monsoon: Its relation with time variation of monsoon rainfall, *Mon. Weather Rev.*, *121*, 2465–2482.

Chu, P.-S. (1988), Extratropical forcing and the burst of equatorial westerlies in the western Pacific, *J. Meteorol. Soc. Jpn.*, *66*, 549–563.

Chu, P.-S., and J. Frederick (1990), Westerly wind bursts and surface heat fluxes in the equatorial western Pacific in May 1982, *J. Meteorol. Soc. Jpn.*, *68*, 523–536.

Compo, G. P., G. N. Kiladis, and P. J. Webster (1999), The horizontal and vertical structure of east Asian winter monsoon pressure surges, *Q. J. R. Meteorol. Soc.*, *125*, 29–54.

Fukutomi, Y., and T. Yasunari (2005), Southerly surges on submonthly time scales over the eastern Indian Ocean during the southern hemisphere winter, *Mon. Weather Rev.*, *77*, 1637–1654.

Goswami, B. N., and R. S. Ajaya Mohan (2001), Intraseasonal oscillations and interannual variability of the Indian summer monsoon, *J. Clim.*, *14*, 1180–1198.

Han, W., W. T. Liu, and J. Lin (2006), Impact of atmospheric submonthly oscillations on sea surface temperature of the tropical Indian Ocean, *Geophys. Res. Lett.*, *33*, L03609, doi:10.1029/2005GL025082.

Hartten, L. M. (1996), Synoptic settings of westerly wind bursts, *J. Geophys. Res.*, *101*(D12), 16,997–17,019.

Kaylor, R. E. (1977), Filtering and decimation of digital time series, *Tech. Note BN 850*, 42 pp., Inst. of Phys. Sci. and Technol., Univ. of Maryland, College Park.

Kiladis, G. N., and M. Wheeler (1995), Horizontal and vertical structure of observed tropospheric equatorial Rossby waves, *J. Geophys. Res.*, *100*(D11), 22,981–22,997.

Kiladis, G. N., G. A. Meehl, and K. M. Weickmann (1994), Large-scale circulation associated with westerly wind bursts and deep convection over the western equatorial Pacific, *J. Geophys. Res.*, *99*(D9), 18,527–18,544.

Kummerow, C., et al. (2000), The status of the tropical rainfall measuring mission (TRMM) after two years in orbit, *J. Appl. Meteorol.*, *39*, 1965–1982.

Lim, H., and C.-P. Chang (1981), A theory of midlatitude forcing of tropical motions during winter monsoons, *J. Atmos. Sci.*, *38*, 2377–2392.

Love, G. (1985a), Cross-equatorial influence of winter hemisphere subtropical cold surges, *Mon. Weather Rev.*, *113*, 1487–1498.

Love, G. (1985b), Cross-equatorial interactions during tropical cyclogenesis, *Mon. Weather Rev.*, *113*, 1499–1509.

Masumoto, Y., H. Hase, Y. Kuroda, H. Matsuura, and K. Takeuchi (2005), Intraseasonal variability in the upper layer currents observed in the eastern equatorial Indian Ocean, *Geophys. Res. Lett.*, *32*, L02607, doi:10.1029/2004GL021896.

Masumoto, Y., T. Horii, I. Ueki, H. Hase, K. Ando, and K. Mizuno (2008), Short-term upper-ocean variability in the central equatorial Indian Ocean during 2006 Indian Ocean Dipole event, *Geophys. Res. Lett.*, *35*, L14S09, doi:10.1029/2008GL033834.

Matsuno, T. (1966), Quasi-geostrophic motions in the equatorial area, *J. Meteorol. Soc. Jpn.*, *44*, 25–43.

Meehl, G. A., G. N. Kiladis, K. M. Weickmann, M. Wheeler, D. S. Gutzler, and G. P. Compo (1996), Modulation of equatorial subseasonal convective episodes by tropical-extratropical interaction in the Indian and Pacific Ocean regions, *J. Geophys. Res.*, *101*(D10), 15,033–15,049.

Murakami, T. (1988), Equatorward surges, equatorial westerlies and convection on interannual and intraseasonal time scales, *UHMET 88-02*, 18 pp., Dept. of Meteorol., Univ. of Hawaii, Honolulu.

Murakami, T., and W. L. Sumathipala (1989), Westerly bursts during the 1982/83 ENSO, *J. Clim.*, *2*, 71–85.

Murakami, T., and A. Sumi (1981), Large-scale aspects of the 1978–79 winter circulation over the greater WMONEX region. Part II: Long-period perturbations, *J. Meteorol. Soc. Jpn.*, *59*, 646–671.

Ogata, T., H. Sasaki, V. S. N. Murty, M. S. S. Sarma, and Y. Masumoto (2008), Intraseasonal meridional current variability in the eastern equatorial Indian Ocean, *J. Geophys. Res.*, *113*, C07037, doi:10.1029/2007JC004331.

Onogi, K., et al. (2005), JRA-25; Japanese 25-year reanalysis—Progress and status, *Q. J. R. Meteorol. Soc.*, *131*, 3259–3268.

Onogi, K., et al. (2007), The JRA-25 analysis, *J. Meteorol. Soc. Jpn.*, *85*, 369–432.

Pires, P., J.-L. Redelsperger, and J.-P. Lafore (1997), Equatorial atmospheric waves and their association to convection, *Mon. Weather Rev*, *125*, 1167–1184.

Plumb, R. A. (1986), Three-dimensional propagation of transient quasi-geostrophic eddies and its relationship with the eddy forcing of the time-mean flow, *J. Atmos. Sci.*, *56*, 1657–1678.

Sengupta, D., R. Senan, and B. N. Goswami (2001), Origin of intraseasonal variability of circulation in the tropical central Indian Ocean, *Geophys. Res. Lett.*, *28*(7), 1267–1270.

Sengupta, D., R. Senan, V. S. N. Murty, and V. Fernando (2004), A biweekly mode in the equatorial Indian Ocean, *J. Geophys. Res.*, *109*, C10003, doi:10.1029/2004JC002329.

Shinoda, T., and W. Han (2005), Influence of the Indian Ocean Dipole on atmospheric subseasonal variability, *J. Clim.*, *18*, 3891–3909.

Shrestha, M. L., and T. Murakami (1988), Intraseasonal fluctuations in low-level meridional winds over the Indian Ocean and monsoonal convection over South Asia, *Tellus, Ser. A*, *40*, 120–132.

Sobel, A. H., and C. S. Bretherton (1999), Development of synoptic-scale disturbances over the summertime tropical northwest Pacific, *J. Atmos. Sci.*, *56*, 3106–3127.

Sobel, A. H., and E. D. Maloney (2000), Effect of ENSO and the MJO on western North Pacific tropical cyclones, *Geophys. Res. Lett.*, *27*(12), 1739–1742.

Straub, H. H., and G. N. Kiladis (2003), Extratropical forcing of convectively coupled Kelvin waves during Austral winter, *J. Atmos. Sci.*, *60*, 526–543.

Sumathipala, W. L., and T. Murakami (1988), Intraseasonal fluctuations in low-level meridional winds over the South China Sea and the western Pacific and monsoonal convection over Indonesia and northern Australia, *Tellus, Ser. A*, *40*, 205–219.

Suppiah, R., and X. Wu (1998), Surges, cross-equatorial flows and their links with the Australian summer monsoon circulation and rainfall, *Austral. Meteorol. Mag.*, *47*, 113–130.

Tomas, R. A., and P. J. Webster (1997), On the location of the intertropical convergence zone and near-equatorial convection: The role of inertial instability, *Q. J. R. Meteorol. Soc.*, *123*, 1445–1482.

Trenberth, K. E. (1986), An assessment of the impact of transient eddies on the zonal flow a blocking episode using localized Eliassen-Palm flux diagnostics, *J. Atmos. Phys.*, *43*, 2070–2087.

Wang, X.-L., and T. Murakami (1987), Intraseasonal meridional surges and equatorial convections during the Southern Hemisphere summer, *J. Meteorol. Soc. Jpn.*, *65*, 727–736.

Yokoi, S., and T. Satomura (2005), An observational study of intraseasonal variations over southeast Asia during the 1998 rainy season, *Mon. Weather Rev.*, *133*, 2091–2104.

Yokoi, S., and T. Satomura (2006), Mechanisms of the northward movement of submonthly scale vortices over the bay of Bengal during the boreal summer, *Mon. Weather Rev.*, *134*, 2265–2551.

Yu, L., and M. M. Rienecker (1998), Evidence of an extratropical influence during the onset of 1997–1998 El Nino, *Geophys. Res. Lett.*, *25*(18), 3537–3540.

Yu, L., R. Weller, and W. T. Liu (2003), Case analysis of a role of ENSO in regulating the generation of westerly wind bursts in the western equatorial Pacific, *J. Geophys. Res.*, *108*(C4), 3128, doi:10.1029/2002JC001498.

Zhang, C., and P. J. Webster (1992), Laterally forced equatorial perturbations in a linear model: Part I. Stationary transient forcing, *J. Atmos. Sci.*, *49*, 585–607.

Y. Fukutomi, Frontier Research Center for Global Change, Japan Agency for Marine-Earth Science and Technology, 3173-25 Showamachi, Kanazawa-ku, Yokohama, Kanagawa 236-0033, Japan. (fukutomi@jamstec.go.jp)

T. Yasunari, Hydrospheric Atmospheric Research Center, Nagoya University, Furo-cho, Chikusa-ku, Nagoya, Aichi 464-8601, Japan. (yasunari@hyarc.nagoya-u.ac.jp)